Ohmic friction at the transition from laminar to turbulent pipe flow

Rudolf Jaggi [a)]

Apartado 1140, 8700 Olhão, Portugal

The classical Navier-Stokes equation is extended by an Ohmic friction term proportional to $\mathbf{v}$ depending on the adherence lengths $\lambda_A = 1/\alpha$ and $\lambda_B = 1/\beta$ for eddy-free and turbulent flow, respectively. Laminar Hagen-Poiseuille flow is laminar with $\alpha = 0$. For α finite is the novel category of hyperlaminar flow valid in the whole range of Reynolds numbers $Re = Re_D/2$. In circular pipes of radius $a = D/2$ are axisymmetric effective velocities v solutions of a Bessel differential equation in agreement with Reynolds' original experiments and with recent measurements. $Re = Re_\alpha = 1000$ is the lowest critical Reynolds number, where $\lambda_A = a$, $\alpha a = 1$. For $Re < Re_\alpha$ is the hyperlaminar flow is determined by $\lambda_A > a$, $\alpha a < 1$. For $Re > Re_\alpha$ is the hyperlaminar $\lambda_A < a$, $\alpha a > 1$; the turbulent flow is characterized by $\lambda_B < \lambda_A$, $\beta a > \alpha a$. In summary, the transition process consists in the change of the adherence length from λ_A to λ_B. The Appendix presents a comparison of the logarithmic velocity law with the effective velocities.

Keywords: Navier-Stokes equation, velocity profiles, transition to turbulence

---

a) Retiree of IBM Research – Zurich, Rüschlikon, Switzerland, and Universidade do Algarve, Faro, Portugal.
Email address for correspondence: jaggi.rudolf@yahoo.com.

I. INTRODUCTION

Osbourne Reynolds' famous pipe flow experiments[1] are still subject of numerous investigations. The transition from laminar to turbulent flow is treated in various publications, e. g. in books by Schlichting and Gersten

[2] and by White,[3] whereas topical reviews of different aspects have been written by Kerswell,[4] Willis et al.,[5] Mullin,[6] and Kim.[7]

In appreciation of the foregoing research, a novel effective velocity distribution as alternative to the classical logarithmic velocity law will be presented by the following paradigm.

II. NAVIER-STOKES FLUIDDYNAMICS AND OHMIC FRICTION

The basis is the classical Navier-Stokes momentum equation extended by the addition of an '*Ohmic*' friction term $\mathbf{\Omega}$ proportional to $\mathbf{v}$

$$\varrho\frac{D\mathbf{v}}{Dt} = \mu\Delta\mathbf{v} + \varrho\mathbf{g} - \nabla p - \mathbf{\Omega}\,. \tag{1}$$

The notation is as usual[2,3] with $\mathbf{v}$ the velocity**,** $\mathbf{g}$ the acceleration of gravity, p the pressure, including the two material properties, the density ϱ and the viscosity μ or the kinematic viscosity $\nu = \mu/\varrho$, disregarding inviscid flows. Continuity is *strict* $\nabla\mathbf{v} = 0$ for incompressible fluids inside smooth walls in thermodynamic equilibrium. The total acceleration is the sum of the local acceleration and the convection:

$$\frac{D\mathbf{v}}{Dt} = \frac{\partial\mathbf{v}}{\partial t} + (\mathbf{v}\nabla)\mathbf{v}\,. \tag{2}$$

In Electrodynamics is the frictional force proportional to the velocity $\mathbf{v}$ of the electron fluid fundamental for the electric current in normal conductors and Ohm's law. Benthem and Kronig[8] included in the equation of motion the Laplace term $\mu\Delta\mathbf{v}$. The resulting differential

equation was applied to the anomalous skin effect [8] and to the dc size effect [9] in agreement with experiments.

The unity of Physics requires for Fluiddynamics of ordinary fluids also a friction force proportional to the velocity $\mathbf{v}$. We introduce the Ohmic friction force density in the form

$$\mathbf{\Omega} = \mu\alpha^2\mathbf{v} \tag{3}$$

with $\alpha = 1/\lambda_A$. The characteristic *adherence length* λ_A serves as a measure for the adherence of the fluid at the wall with regard to the non-slip condition $\mathbf{v}_{wall} = 0$ and the local velocity distribution.

Specifically, for steady horizontal pipe flows, we restrict ourselves to a one-dimensional calculus where continuity is guaranteed and the omission of convection is correct. Thus from equation (1) remains the stationary extended Navier-Stokes equation [10]

$$\Delta\mathbf{v} - \alpha^2\mathbf{v} = \frac{1}{\mu}\nabla p\,. \tag{4}$$

The normalized hyperlaminar adherence length of fully developed pipe flows, $\lambda_A/a = 1/\alpha a$, is a function $f(Re)$ of the classical Reynolds number

$$Re = \frac{\varrho a v_{ave}}{\mu} = \frac{a v_{ave}}{\nu}\left[= \frac{Re_D}{2}\ \text{s. v. factor}\ \frac{1}{2}\right], \tag{5}$$

originally defined [1] with radius $r = a = D/2$.

The efficient averaging procedure v_{ave} = volume rate Q divided by the cross-section πa^2 is of general significance concerning the Reynolds numbers for flows of all kinds in experiment and theory.

The second-order differential equation (4) has the great advantage being linear in $\mathbf{v}$ which on its part is a function of αr; it is valid in the entire range of Re, also for turbulent flows, in the latter case by substitution of $\beta = 1/\lambda_B$ for $\alpha = 1/\lambda_A$.

III. PROFILES OF THE EFFECTIVE VELOCITY $v_z(r)$

We consider the axial flow in a circular pipe of radius a, length $L \gg a$ and applied pressure p_A. In appropriate cylindrical coordinates (r, z) with the *effective velocity* $v_z(r)$ and the constant pressure gradient $\partial p/\partial z = -p_A/L$ follows from the stationary equation of motion (4) the inhomogeneous Bessel differential equation of zeroth order

$$\frac{d^2 v_z}{dr^2} + \frac{1}{r}\frac{dv_z}{dr} - \alpha^2 v_z = -\frac{1}{\mu}\frac{p_A}{L}. \tag{6}$$

Physics demands that the axi-symmetric problem has the even solution fulfilling the non-slip boundary conditions

$$v_z(r) = \frac{1}{\mu\alpha^2}\frac{p_A}{L}\left\{1 - \frac{I_0(\alpha r)}{I_0(\alpha a)}\right\}, \quad r = \pm a \quad v_z(\pm a) = 0. \tag{7}$$

$$I_0(\alpha r) = J_0(i\alpha r) = 1 + \frac{\alpha^2 r^2}{4} + \frac{\alpha^4 r^4}{64} + \ldots \text{ and}$$

$$I_1(\alpha r) = -iJ_1(i\alpha r) = \frac{\alpha r}{2}\left(1 + \frac{\alpha^2 r^2}{8} + \frac{\alpha^4 r^4}{192} + \ldots\right) \tag{8}$$

are the modified Bessel functions of the zeroth and first orders, respectively.

Knowing the velocity $v_z(r)$ (7) we can calculate all features of interest explicitly. At first the important average velocity

$$v_{ave} = \frac{Q}{\pi a^2} = \frac{1}{\pi a^2} 2\pi \int_{r=0}^{a} r v_z(r) dr = \frac{1}{\mu\alpha^2}\frac{p_A}{L}\Phi_A(\alpha a) = \frac{v}{a} Re \tag{9}$$

where the *fluiddynamic conduction function*

$$\Phi_A(\alpha a) = 1 - \frac{2}{\alpha a}\frac{I_1(\alpha a)}{I_0(\alpha a)}. \tag{10}$$

By natural normalization $V_z(\xi)=\frac{v_z(r)}{v_{ave}}$, $\xi=\frac{r}{a}$ and $\alpha r=\alpha a\xi$ results from equation (6) the dimension-less Bessel differential equation

$$\frac{d^2V_z}{d\xi^2}+\frac{1}{\xi}\frac{dV_z}{d\xi}-\alpha^2a^2V_z=-\frac{\alpha^2a^2}{\Phi_A(\alpha a)}. \tag{11}$$

The solution is for $0\le\alpha a\le\infty$

$$V_z(\xi)=\frac{1}{\Phi_A(\alpha a)}\left\{1-\frac{I_0(\alpha a\xi)}{I_0(\alpha a)}\right\},\ \xi=\pm1\ V_{wall}=0, \tag{12}$$

$$\frac{dV_z(\xi)}{d\xi}=-\frac{\alpha a}{\Phi_A(\alpha a)}\frac{I_1(\alpha a\xi)}{I_0(\alpha a)},\ \xi=0\ \left(\frac{dV_z}{d\xi}\right)_{axis}=0, \tag{13}$$

$$\frac{d^2V_z(\xi)}{d\xi^2}=-\frac{\alpha^2a^2}{\Phi_A(\alpha a)}\left\{\frac{I_0(\alpha a\xi)}{I_0(\alpha a)}-\frac{1}{\alpha a\xi}\frac{I_1(\alpha a\xi)}{I_0(\alpha a)}\right\}<0,\ V_z(\xi)\ \text{convex}. \tag{14}$$

Figure 1 shows the actual symmetric profiles of the normalized effective velocity $V_z(\xi)$. The profile for $\alpha a=0$ corresponds to the well known Hagen-Poiseuille paraboloid

$$V_z(\xi)=2\left\{1-\xi^2\right\} \tag{15}$$

where $V_{max}=2$. The special case $\alpha a=1$ is nearby with $V_{max}=1.960$. For higher values of αa the profiles will become increasingly steeper near the wall and flatter near the axis. For $\alpha a\gg1$ the profile is becoming uniform. In the extreme $\alpha a\to\infty$ is $V_z=1$.

A direct experimental realization of figure 1 is Nakayama's beautiful hydrogen-bubble visualization of flow in the entrance of a tube [Fig. 1 – 11 of Ref. 3].

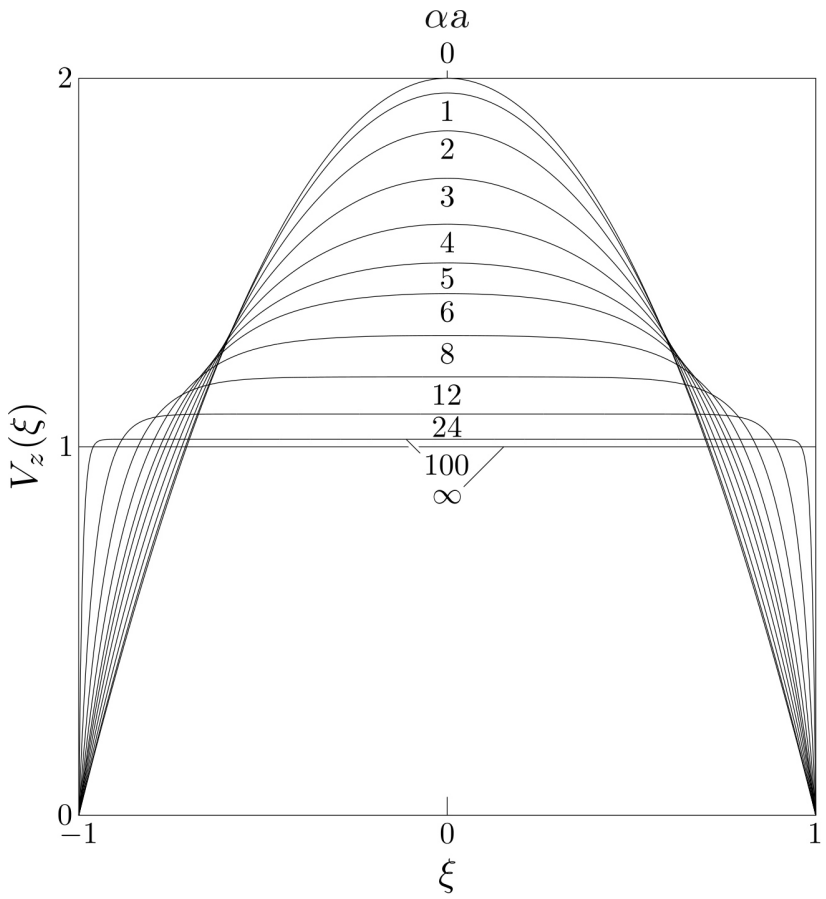

FIG. 1. Profiles of the normalized effective velocity $V_z(\xi)$ vs. ξ with parameters αa.

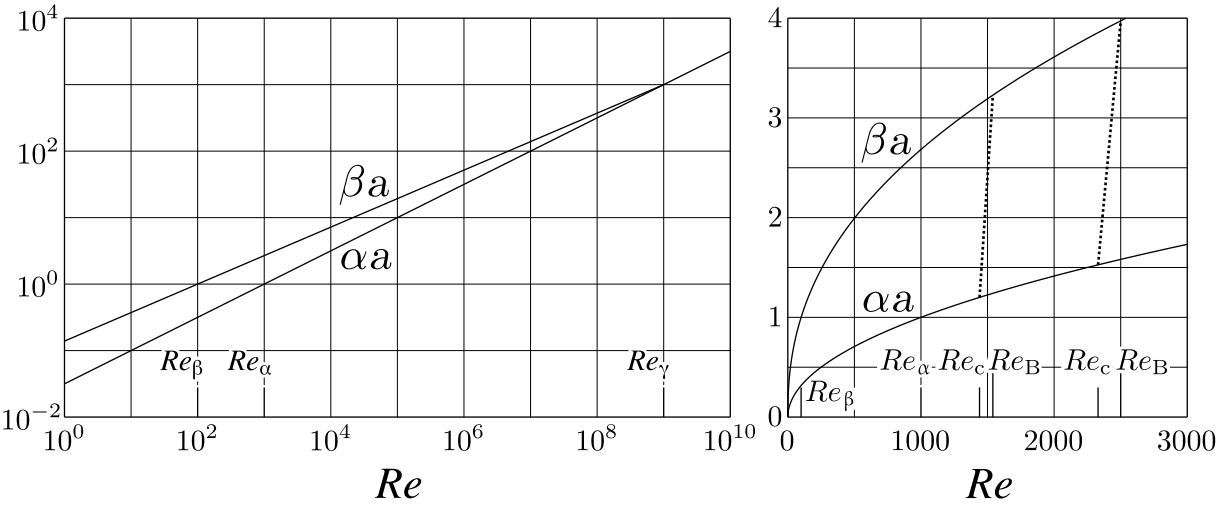

FIG. 2. Reciprocal normalized adherence lengths $\alpha a = a/\lambda_A$ and $\beta a = a/\lambda_B$ vs. Re with two Oregon transitions, in logarithmic axes and in linear axes.

IV. LAMINAR, HYPERLAMINAR AND TURBULENT FLOW

For $\alpha a = 0$ ist the Hagen-Poiseuille flow (15) solution of equation (11). We reserve the notion '*laminar*' for the case $\alpha a = 0$. For αa finite we propose the novel category of '*hyperlaminar flow*'.

In the limit of $\alpha a \gg 1$, according to figure 1, the flow is becoming uniform independent of r, with velocity $v_z = v_{ave} = Re\, v/a$. Therefore the differential equation (6) is reduced to

$$\alpha^2 v_z = \frac{1}{\varrho v}\frac{p_A}{L}, \tag{16}$$

$$\alpha^2 a^2 Re = \frac{a^3}{\varrho v^2 L} p_A = P_{AH}. \tag{17}$$

The normalized pressure P_{AH} has to be proportional to Re^2. We define the hyperlaminar

$$\alpha a = \left(\frac{Re}{Re_\alpha}\right)^{k_\alpha} \tag{18}$$

with the exponent $k_\alpha = \frac{1}{2}$, the hyperlaminar reference $Re_\alpha = 1000$ is the lowest critical Reynolds number (see Section V).

The differential equations (6) and (11) are valid for turbulent velocities too, simply by replacing αa for fully developed flows by

$$\beta a = \left(\frac{Re}{Re_\beta}\right)^{k_\beta} \tag{19}$$

with the exponent $k_\beta = \frac{3}{7}$ and the turbulent reference $Re_\beta = 100$. The definitions (18) and (19) yield agreement with the experiments.

Figure 2 presents αa and βa up to $Re = 10^{10}$. Note in the logarithmic plot $k_\alpha = \frac{3}{6}$ and $k_\beta = \frac{3}{7}$. At $Re = Re_\alpha$ is $\alpha a = 1$ and $\beta a = 2.683$. In the linear plot two Oregon transitions are indicated, where αa as the *first critical Reynolds number* $Re_C = Re_{crit}$ changes to βa at the *second critical Reynolds number* Re_B. Numerical values have been collected in Table I, Section VIII.

For $Re \gg Re_\alpha$ is βa approximating to αa reaching equality $\beta a = \alpha a = 10^3$ at $Re = Re_\gamma = 10^9$. Here we predict the finale of the turbulent pipe flow and the continuation of the hyperlaminar flow, with the necessary caution for such enormous Reynolds numbers.

V. FLOW PROPERTIES

A. Hyperlaminar flow

Properties of the hyperlaminar flow are in detail:

the maximum velocity

$$V_{max} = V_z(0) = \frac{1}{\Phi_a(\alpha a)}\left\{1 - \frac{1}{I_0(\alpha a)}\right\}; \tag{20}$$

the pressure

$$p_A = \frac{\varrho v^2 L}{a^3}\frac{1}{\Psi_A(\alpha a)}Re; \tag{21}$$

the *norm pressure*

$$p_N = \frac{\varrho v^2 L}{a^3}, \tag{22}$$

$p_N = 1\,\text{Pascal}$ for water at room temperature with $a = 1\,\text{mm}$ and $L = 1\,\text{m}$;

the *fluiddynamic conductivity*

$$\Psi_{\mathrm{A}}(\alpha a)=\frac{\Phi_{\mathrm{A}}(\alpha a)}{\alpha^2 a^2};\tag{23}$$

the normalized pressure $\frac{p_{\mathrm{A}}}{p_{\mathrm{N}}}=$

$$P_{\mathrm{A}}=\frac{1}{\Psi_{\mathrm{A}}(\alpha a)}Re\tag{24}$$

analogous to Ohm's law of Electrodynamics

$$E=\frac{1}{\sigma(\alpha_{\mathrm{el}}a)}J\,,\tag{25}$$

where E is the electric field, $\sigma(\alpha_{\mathrm{el}}a)$ the electric conductivity, and J the current density;

the *norm kinetic energy* pro volume

$$e_{\mathrm{N}}=\frac{\varrho}{2}v_{\mathrm{ave}}^2=\frac{\varrho}{2}\frac{v^2}{a^2}Re^2;\tag{26}$$

the friction factor, defined with pressure $p_{\mathrm{A}}(Re)$

$$\Lambda_{\mathrm{A}}(Re)=\frac{2a}{L}\frac{p_{\mathrm{A}}(Re)}{e_{\mathrm{N}}}=\frac{4}{Re}\frac{1}{\Psi_{\mathrm{A}}(\alpha a)};\tag{27}$$

the *fluiddynamic conductance*

$$G_{\mathrm{A}}(Re)=1/\Lambda_{\mathrm{A}}(Re)\,,\tag{28}$$

$$G_{\mathrm{A}}=\frac{L}{2a}\frac{e_{\mathrm{N}}}{p_{\mathrm{A}}}=\frac{Re}{4}\Psi_{\mathrm{A}}(\alpha a)=250\,\Phi_{\mathrm{A}}(\alpha a);\tag{29}$$

the universal relation between conductance and pressure

$$G(Re)\,P(Re)=G_{\mathrm{A}}P_{\mathrm{A}}=Re^2/4\,.\tag{30}$$

Illuminating are the limits of the flow properties.

B. Limit $\alpha a \ll 1$, Hagen-Poiseuille flow as approximation

By series expansion of the Bessel functions (8) is

$$\Phi_{\mathrm{A}}(\alpha a)=\frac{\alpha^2 a^2}{8}\left(1-\frac{\alpha^2 a^2}{6}\pm\ldots\right), \tag{31}$$

subsequently αa disappears from the exact solutions (12 to 26), and we obtain the well known formulas of the dimensional Hagen-Poiseuille-flow as approximations.

$$v_{\mathrm{z}}(r)=2v_{\mathrm{ave}}\left\{1-\frac{r^2}{a^2}\right\}: \tag{32}$$

the maximum velocity

$$v_{\max}=v_{\mathrm{z}}(0)=2v_{\mathrm{ave}}=\frac{1}{4}\frac{a^2}{\mu}\frac{p_{\mathrm{AL}}}{L}; \tag{33}$$

the average velocity

$$v_{\mathrm{ave}}=\frac{1}{8}\frac{a^2}{\mu}\frac{p_{\mathrm{AL}}}{L}=\frac{v}{a}Re; \tag{34}$$

the pressure

$$p_{\mathrm{AL}}=8\frac{\mu L}{a^2}v_{\mathrm{ave}}=8p_{\mathrm{N}}Re; \tag{35}$$

the normalized pressure

$$\frac{p_{\mathrm{AL}}}{p_{\mathrm{N}}}=P_{\mathrm{AL}}=8Re; \tag{36}$$

the friction factor

$$\Lambda=\frac{32}{Re}\left[=\frac{64}{Re_{\mathrm{D}}}\right]; \tag{37}$$

the conductance

$$G_{\mathrm{AL}}=\frac{Re}{32}; \tag{38}$$

the GP relation

$G_{\mathrm{AL}}P_{\mathrm{AL}}=Re^2/4$ (30).

C. Limit $\alpha a \gg 1$, hyperlaminar flow

For the eddy-free unidirectional flow with $Re \geq Re_\alpha$, $\alpha a \geq 1$, we propose the new category of '*hyperlaminar flow*'. Then for $Re < Re_\alpha$, $\alpha a < 1$, the flow is '*laminar*' in a closer sense.

In the extreme $\alpha a \to \infty$, the flow is uniform and independent of r, with velocity $v_z = v_{ave} = Re\, \nu / a$. Therefore the differential equation (6) is reduced to $p_{AH} / p_N = P_{AH} = Re\, \alpha^2 a^2$, which has to be proportional to Re^2 by extrapolation. We define, for fully developed flows,

$$\alpha^2 a^2 = \frac{Re}{Re_\alpha} = \frac{Re}{1000} \tag{39}$$

with the '*standard Reynolds number*' $Re_\alpha = 1000$, a round value that is adequate for the present approach.

The hyperlaminar flow obeys the equations (12) to (26), asymptotic solutions are:

the conduction function

$$\Phi_{AH} = 1; \tag{40}$$

the conductivity

$$\Psi_{AH} = \frac{1}{\alpha^2 a^2} = \frac{Re_\alpha}{Re} = \frac{1000}{Re}; \tag{41}$$

the normalized pressure

$$P_{AH} = Re\, \alpha^2 a^2 = \frac{Re^2}{Re_\alpha} = \frac{Re^2}{1000}; \tag{42}$$

the conductance

$$G_{\mathrm{AH}} = \frac{1}{4}\frac{Re}{\alpha^2 a^2} = \frac{Re_\alpha}{4} = 250\,; \tag{43}$$

the GP relation

$G_{\mathrm{AH}} P_{\mathrm{AH}} = Re^2 / 4$ (27).

D. Turbulent flow

The turbulent properties, with their extrapolations for $\beta a \gg 1$ are:

the conduction function

$$\Phi_{\mathrm{B}}(\beta a) = 1 - \frac{2}{\beta a}\frac{I_1(\beta a)}{I_0(\beta a)},\ \Phi_{\mathrm{BH}} = 1; \tag{44}$$

the conductivity

$$\Psi_{\mathrm{B}}(\beta a) = \frac{\Phi_{\mathrm{B}}(\beta a)}{\beta^2 a^2},\ \Psi_{\mathrm{BH}} = \frac{1}{\beta^2 a^2}; \tag{45}$$

the normalized pressure

$$P_{\mathrm{B}} = \frac{Re}{\Psi_{\mathrm{B}}(\beta a)},\ P_{\mathrm{BH}} = Re\,\beta^2\alpha^2; \tag{46}$$

the conductance

$$G_{\mathrm{B}} = \frac{Re}{4}\Psi_{\beta}(\beta a),\ G_{\mathrm{BH}} = \frac{1}{4}\frac{Re}{\beta^2 a^2}; \tag{47}$$

the GP relation

$\mathrm{G_B P_B} = \mathrm{G_{BH} P_{BH}} = Re^2 / 4$ (27).

VI. REYNOLDS' PIPE FLOW EXPERIMENTS

Reynolds[1] performed two sets of experiments. The first one is shown in his famous three figures [page 942 of Ref. 1]. Glass tubes (1 inch, ½ inch, and ¼ inch in diameter), having rounded inlets and smooth walls, are immersed in a large tank. The carefully controlled undisturbed water is entering the tubes with an axial band-shaped color dye marker. The steady

flow is uniform at the entrance $z = 0$ with average velocity $v_{ave} = Re\ \nu/a$ (9) and norm kinetic energy $e_N = \frac{\varrho}{2} v_{ave}^2$ (22) due to the applied pressure gradient $\partial p/\partial z = -p_A/L$.

To be brief in the case of small Re: Within the distance $z = z_{AL}$, the Hagen-Poiseuille profile $v_z(r)$ (29) is formed, for which the kinetic energy pro volume increases to

$$e_{kin} = \frac{2}{a^2} \int_{r=0}^{a} \frac{\varrho}{2} v_z^2(r)\, r\, dr = \frac{4}{3} \frac{\varrho}{2} v_{ave}^2 = \frac{4}{3} e_N . \tag{48}$$

We suppose that the increase of kinetic energy compensates the decrease of pressure.

$$\frac{1}{3} e_N = p_{AL} \frac{z_{AL}}{L} . \tag{49}$$

With p_N (18), e_N (22) and p_{AL} (32) we obtain the normalized entrance length for small Re

$$\frac{z_{AL}}{a} = \frac{Re}{48}, \quad \alpha a \ll 1 . \tag{50}$$

More in detail for all Re: With $V_z(\xi)$ (12) is the normalized hyperlaminar kinetic energy

$$E_A(\alpha a) = \frac{e_{kin}(\alpha a)}{e_N} = 2 \int_{\xi=0}^{1} V_z^2(\xi)\, \xi\, d\xi = \frac{2\Phi_A(\alpha a) - \frac{I_1^2(\alpha a)}{I_0^2(\alpha a)}}{\Phi_A^2(\alpha a)} . \tag{51}$$

We confirm $E_A = 4/3$ and $E_A = 1$ for $\alpha a \ll 1$ and $\alpha a \gg 1$, respectively. At $z = 0$ the uniform velocity v_{ave} corresponds to $\alpha a \to \infty$; with increasing z the undeveloped αa decreases like in figure 1. The flow is fully developed with $\alpha a = (Re/Re_\alpha)^{1/2}$ and $E_A(\alpha a)$ at $z = z_A$. Analogous to equation (49) the kinetic energy difference is compensated by a pressure difference,

$$e_N \left(E_A(\alpha a) - 1 \right) = p_N P_A(\alpha a) \frac{z_A(\alpha a)}{L} . \tag{52}$$

With P_A (20), G_A (26) and E_A (52) results the normalized entrance length

$$\frac{z_{\mathrm{A}}(\alpha a)}{a} = 2G_{\mathrm{A}}(\alpha a)\left(E_{\mathrm{A}}(\alpha a) - 1\right) \tag{53}$$

[$z_{\mathrm{A}} = 0$ for $Re = 0$ and $Re \to \infty$ smaller than former expectations [3,12]].

In the limit of small Re, $\alpha a \ll 1$, we confirm z_{AL}/a (50). For stable laminar flow $Re < Re_{\alpha}$ Nakayama's visualization for $Re = 800$, $\alpha a = 0.894$, allows a rough estimate $z_{\mathrm{A}}/a = 14 \pm 2$, while equation (53) yields $z_{\mathrm{A}}/a = 14.2$. For $Re = 1.543 \times 10^4$, $\alpha a = 3.928$, is the *maximum* $z_{\mathrm{A}}/a = 59.77$. Reynolds mentions a value of about 60 for Re of the order of 1×10^4. For $Re = 1.94 \times 10^5$, $\alpha a = 13.93$, Barbin's entry length value $z_{\mathrm{A}}/a = 30$ [quoted from Ref. 12] can be compared with $z_{\mathrm{A}}/a = 30.59$ from equation (53).

So far, Reynolds' figure 3 [Ref. 1] with the color band in a straight line shows the eddy-free situation where thanks to favorable entrance conditions, hyperlaminar flow can persist up to high Re. But the hyperlaminar flow is not stable. In Reynolds' figures 4 and 5, the color band mixes with the water showing eddies at a considerable distance $z = z_{\mathrm{A}}$ from the intake for the first critical Reynolds number Re_{crit}. After the onset of turbulence, the hyperlaminar αa changes as a result of fluctuating transition mechanisms to the turbulent βa for the second critical Reynolds number Re_{B}, reaching the turbulent kinetic energy

$$E_{\mathrm{B}}(\beta a) = \frac{2\Phi_{\mathrm{B}}(\beta a) - \dfrac{\mathrm{I}_1^2(\beta a)}{\mathrm{I}_0^2(\beta a)}}{\Phi_{\mathrm{B}}^2(\beta a)} \tag{54}$$

which is smaller than the hyperlaminar kinetic energy $E_{\mathrm{A}}(\alpha a)$ (51) .With $G_{\mathrm{B}} < G_{\mathrm{A}}$ results the turbulent entrance length

$$\frac{z_{\mathrm{B}}(\beta a)}{a} = 2G_{\mathrm{B}}(\beta a)\left(E_{\mathrm{B}}(\beta a) - 1\right) \tag{55}$$

which is smaller than z_A/a.

The entrance of turbulence takes place closer to the intake in accordance with Reynolds observations. It is clear that the entrance lengths decreases towards zero for $Re \to \infty$.

In the second setup of experiments, quarter-inch and half-inch lead pipes were used. The water entering from the Manchester mean was on purpose highly disturbed, in contrast to the first setup. Reynolds plotted the measured pressure-velocity relation on a logarithmic scale. For low p he observed, within small experimental uncertainties, linear Hagen-Poiseuille behavior (29) in approximation to the exact laminar relation (7). We have to emphasize that the water was in a state of eddy-full disturbance. In our evaluations of the original data, we see the first inclination changes in the logarithmic P - Re plots at $Re_{crit} = 1003 \pm 10$ and 1028 ± 15.

Within narrow limits, $Re_\alpha = 1000$ is the lowest critical Reynolds number, a round value adequate for the present approach. Reports about $Re_{crit} < 1000$ require special consideration. In the case $Re < Re_\alpha$ it is cruxial that the adherence length λ_A is larger than the radius a, $\alpha a < 1$, for both eddy-free and eddy-full quasi-turbulent flows in smooth and rough walls.

For the fully developed turbulent flows, Reynolds derived the pressure law $p \propto v_{ave}^{1.723}$. In proximity are the Blasius approximation[2,3] $p \propto Re^{1.75}$ and our result $P_B(Re)$ (46).

VII. COMPARISON WITH THE OREGON-PRINCETON EXPERIMENTS

Two pipe flow experiments are combined to provide friction factors for a wide range of Reynolds numbers.[11] In the Princeton Superpipe compressed air is used for $3.13 \times 10^4 \le Re_D \le 3.55 \times 10^7$. In the Oregon device, with examined smooth pipe wall, for $11.2 \le Re_D \le 1.05 \times 10^6$ several room temperature gases are used: helium, nitrogen, oxygen, carbondioxide and sulphurhexafluoride; and at 4.2 K liquid helium. The entrance of the pipe is

first covered by a small screen in the Oregon experiments [Ref. 12]. Upon removal of the screen, the critical Reynolds numbers of carbondioxide and sulphurhexafluoride increased by $60\,\%$, whereas nitrogen and oxygen remained hyperlaminar even at $Re_{\mathrm{D}} = 1.05\times 10^{6}$. Measured are the temperature, the pressure drop p/L, and the mean velocity u_{ave}. Tabulated are the Reynolds number

$$Re_{\mathrm{D}} = \frac{D u_{\mathrm{ave}}}{\nu},\ D = 2a \quad \text{[compare Eq. (5)]}$$

and the friction factor

$$\Lambda = D\frac{p}{L}\Big/\frac{\varrho}{2}u_{\mathrm{ave}}^{2} \quad \text{[compare Eq. (23)].}$$

Reported are experimental errors $2\,\%$ to $4\,\%$ for the Oregon data and $1.1\,\%$ for the Princeton data.

Prandtl derived from the logarithmic velocity law[2,3] (see Appendix) the celebrated formula

$$\frac{1}{\Lambda^{1/2}} = C_1\, log\left(Re_{\mathrm{D}}\,\Lambda^{1/2}\right) - C_2\,. \tag{56}$$

McKeon et al.[11] proposed a curve fit with $C_1 = 1.930$ and $C_2 = 0.537$, which yielded a von Kármán constant $\kappa = 0.421$; the maximum difference between the formula (56) and the Princeton data is always less than $1.25\,\%$.

Comparison of our approach with the Oregon-Princeton experiments is achieved by choosing for each Reynolds number Re the conductance $G = 1/\Lambda$ (origin 0.0), the conductivity $\Psi = 4G/Re$, and the pressure $P = Re/\Psi$, where $GP = Re^{2}/4$ (27). In figure 3, the experimental data for hyperlaminar flow up to $Re = Re_{\mathrm{crit}}$ are plotted together with the solutions P_{A} (20), G_{A} (26) and Ψ_{A} (19), and correspondingly the turbulent data for $Re > Re_{\mathrm{B}}$ together

with the solutions P_B (46), G_B (47), and Ψ_B (45). Within the experimental errors mentioned above, there is agreement almost over the entire range of Reynolds numbers. Differences appear in the linear plots, where between $Re = Re_B$ and $Re \approx 5\times10^4$ the turbulent properties are close to the Blasius approximations $P \propto Re^{7/4}$, $G \propto Re^{1/4}$ [Ref. 6 Fig. 2, Ref. 12 Fig. 6], and $\Psi \propto Re^{-3/4}$. With refernence to figure 2 we realize in figure 3 the intersections $P_A = P_B = 1\times10^{15}$, $G_A = G_B = 250$, $\Psi_A = \Psi_B = 1\times10^{-6}$, and the continuation of the hyperlaminar flow with the necessary caution for such enormous Reynolds numbers.

We know that that turbulence is a rather complex phenomenon. Otherwise we wonder that like Reynolds and McKeon et al. precise and reproducible measurements can be performed whose evaluations lead to simple analytic solutions, what is important for research and engineering.

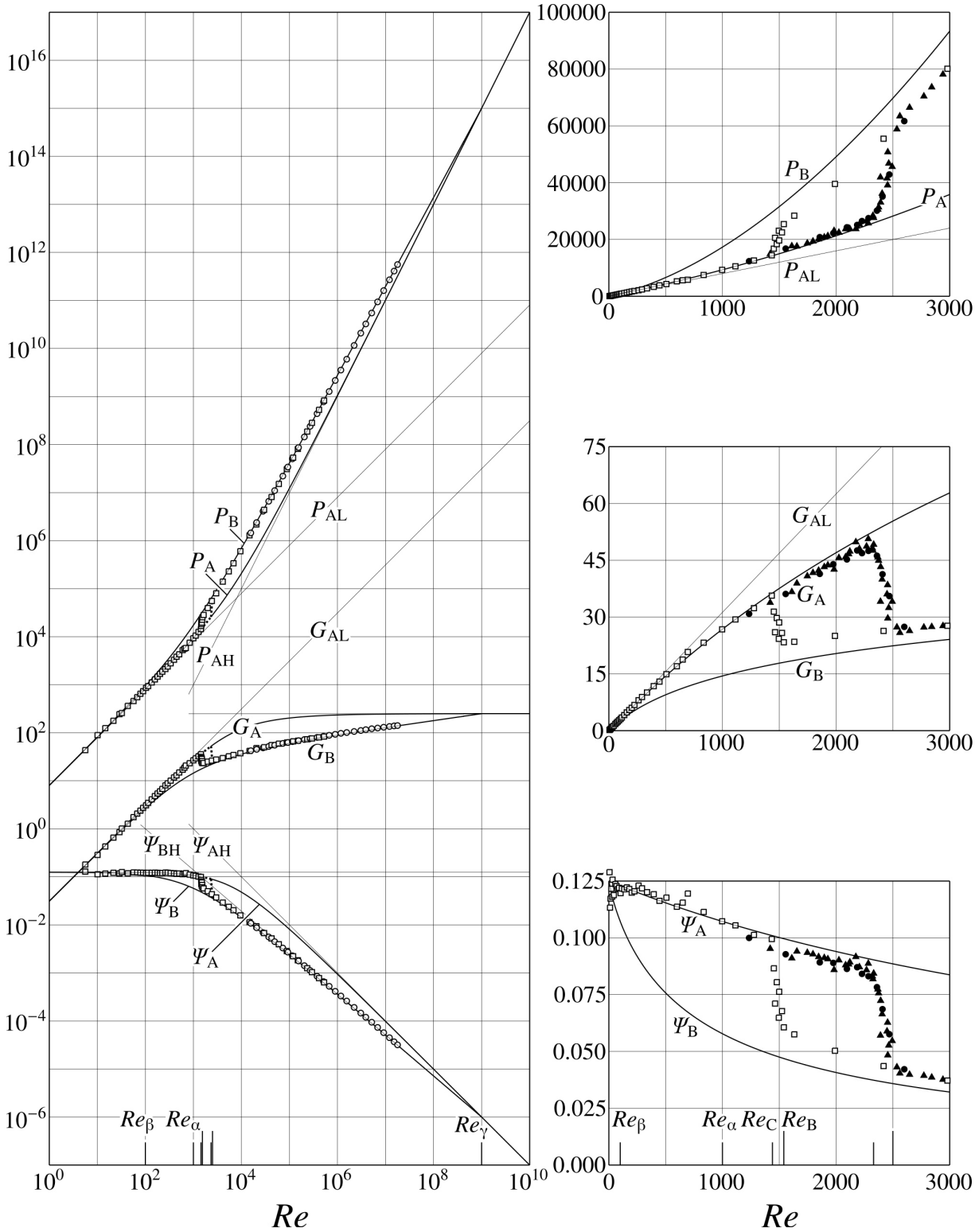

FIG. 3. Pressure P, conductance G, and conductivity Ψ vs. Re, in logarithmic axes and in linear axes.

Experimental data:

◦ air Princeton [11]

▫ He, N_2, O_2, CO_2, SF_6 Oregon screen [11]

▲ CO_2

• SF_6 Oregon no screen [12] author's copy.

VIII. SUMMARY OF THE TRANSITION PROCESS

In the framework of Ohmic friction is the lowest critical Reynolds number $Re = Re_{\alpha} = 1000$ a significant landmark between hyperlaminar and turbulent flow.

If $Re < Re_{\alpha}$, where adherence length λ_A is larger than the radius a, $\alpha a < 1$, no transition to turbulence ever occurs, the hyperlaminar flow obeying equation (7 or 12) is stable to the best of experimental and theoretical knowledge.

If $Re \geq Re_{\alpha}$, $\alpha a \geq 1$, favorable conditions at the entrance $z = 0$ (e.g. carefully rounded inlet, smooth wall and steady undisturbed fluid) allow hyperlaminar flow to continue to high Re, but hyperlaminar flow is not longer stable. Critical entrance conditions (indefinite peculiarities) cause the onset of turbulence to occur after a entrance length z_A for the first critical Reynolds number Re_{crit}, which cannot be predicted exactly. By increasing Re, the hyperlaminar αa changes under fluctuating disturbances to the larger turbulent βa at the smaller entrance length z_B for the second critical Reynolds number Re_B where the turbulent flow is fully developed. The pressure P_B is higher than P_A, and consequently the conductivity Ψ_B, the conductance G_B and the kinetic energy E_B are lower than the respective hyperlaminar values Ψ_A, G_A and E_A. Numerical data of the Oregon experiments are compiled in Table I.

TABLE I. Transition data of the Oregon experiments.

Screen entrance		Open entrance	
$Re_{crit} = 1.440\times10^{3}$	$Re_B = 1.540\times10^{3}$	$Re_{crit} = 2.330\times10^{3}$	$Re_B = 2.500\times10^{3}$
$P_A = 1.427\times10^{4}$	$P_B = 3.157\times10^{4}$	$P_A = 2.580\times10^{4}$	$P_B = 6.673\times10^{4}$
$G_A = 3.634\times10^{1}$	$G_B = 1.878\times10^{1}$	$G_A = 5.261\times10^{1}$	$G_B = 2.341\times10^{1}$
$\Psi_A = 1.009\times10^{-1}$	$\Psi_B = 4.878\times10^{-2}$	$\Psi_A = 9.032\times10^{-2}$	$\Psi_B = 3.746\times10^{-2}$
$E_A = 1.315$	$E_B = 1.243$	$E_A = 1.304$	$E_B = 1.216$
$\alpha a = 1.200$	$\beta a = 3.123$	$\alpha a = 1.526$	$\beta a = 3.846$
$\lambda_A = 1.947$ mm	$\lambda_B = 0.748$ mm	$\lambda_A = 1.530$ mm	$\lambda_B = 0.607$ mm
$z_A = 53.43$ mm	$z_B = 21.28$ mm	$z_A = 74.81$ mm	$z_B = 23.59$ mm
$a = 2.336$ mm	$\frac{\lambda_B}{\lambda_A} = 0.384$		$\frac{\lambda_B}{\lambda_A} = 0.397$

In summary, the transition process consists in the change of the adherence length from λ_A to λ_B.

Supplementary we note in the same spirit: At the exit of any tube we can observe in the unbounded flow a hyperlaminar eddy-free zone of considerable length before turbulence sets in.

IX. OUTLOOK

Generally the complete Navier-Stokes equation (1) permits the computation of multi-dimensional and time-dependent velocities of streams unbounded or in smooth and rough walls, respectively, concerning the phenomenology of Fluiddynamics. The introduction of Ohmic friction with hyperlaminar and turbulent adherence lengths hopefully paves the way to a microscopic explanation of the transition to turbulence.

The application of the linear equation (4) to stationary internal and external flows of different geometries is straightforward. The solutions of four examples shall be given in brevity:

1. In Cartesian coordinates, two parallel planes,[9] $L \gg a$, at $x = \pm a$, boundary condition $v_z(\pm a) = 0$,

$$v_z(x) = \frac{1}{\mu\alpha^2}\frac{p_A}{L}\left\{1 - \frac{\cosh(\alpha x)}{\cosh(\alpha a)}\right\},\ x = 0\ \frac{dv_z}{dx} = 0, \tag{57}$$

$$v_z(x) = \frac{1}{2}\frac{a^2}{\mu}\frac{p_A}{L}\left\{1 - \frac{x^2}{a^2}\right\},\ v_z(0) = v_{max} = \frac{3}{2}v_{ave}\ \text{ laminar } \alpha a \ll 1,$$

analogous to $v_z(r)$ (7 and 29) in cylindrical coordinates.

2. A channel with $v_z(0) = v_0$ at a free surface $x = 0$ over a flat-plate at $x = h$ with $v_z(h) = 0$, in exponential approximation of hyperbolic functions

$$v_z(x) = v_0\{1 - \exp(\alpha x - \alpha h)\}\ \text{ hyperlaminar } \alpha h \gg 1. \tag{58}$$

3. Antisymmetric plane Couette flow, boundary conditions $x = \pm a\ \ v_z(\pm a) = \pm v_a$,

$$v_z(x) = v_a\frac{\sinh(\alpha x)}{\sinh(\alpha a)}, \tag{59}$$

$$v_z(x) = v_a\frac{x}{a}\ \text{ laminar } \alpha a \ll 1.$$

4. Cylindrical symmetries, e. g. the liquid in a rotating cylinder, $L \gg a$, boundary condition $r = a\ \ v_\varphi(a) = \omega a$,

$$v_\varphi(r) = \omega a\frac{I_1(\alpha r)}{I_1(\alpha a)}, \tag{60}$$

$v_\varphi(r) = \omega r$ '*rigid body*' rotation only if $\alpha a \to 0$.

Finally the force per unit length on a cylinder, $L \gg a$, moving in a fluid can be calculated without convection by means of Hankel functions,[10] the problem of Stokes' paradox is avoided thanks to Ohmic friction.

APPENDIX

LOGARITHMIC AND EFFECTIVE VELOCITIES

For turbulent pipe flow derived by dimensional analysis in wall coordinates $y = a - r$, which are adopted from the flat-plate problem, is the one-dimensional logarithmic velocity [2,3]

$$u(y) = u_\tau \left(\frac{1}{\kappa} \ln \frac{u_\tau}{\nu} y + B \right). \tag{A 1}$$

Dimensionless by the wall friction velocity

$$u_\tau = \left(\frac{\tau_{\text{wall}}}{\varrho} \right)^{1/2}, \tag{A 2}$$

originally defined with the wall-shear stress τ_{wall}, is the usual formulation of the classical logarithmic velocity law

$$U^+(Y^+) = \frac{u(y)}{u_\tau} = \frac{1}{\kappa} \ln Y^+ + B, \tag{A 3}$$

$$Y^+ = \frac{u_\tau}{\nu} y = Re^+ \frac{y}{a}, \tag{A 4}$$

$$Re^+ = \frac{a u_\tau}{\nu} = Re \frac{u_\tau}{u_{\text{ave}}}, \tag{A 5}$$

$$\frac{Re^+}{Re} = \frac{u_\tau}{u_{\text{ave}}}, \tag{A 6}$$

κ is the von Kármán constant, B the additive constant.

Omitting several approximations in the near-wall and wake regions, integration in the limits $y = 0$ and $y = a$ yields the average velocity

$$\frac{Q}{\pi a^2} = \frac{1}{\pi a^2} 2\pi \int_{y=0}^{a} (a - y) u(y) \mathrm{d}y, \tag{A 7}$$

$$u_{\text{ave}} = u_\tau \left(\frac{1}{\kappa} \ln \frac{a u_\tau}{\nu} + B - \frac{3}{2\kappa} \right). \tag{A 8}$$

Prandtl derived from this average the famous implicite formula (56) for the friction factor λ; the explicite formula (47) for the conductance $G = 1/\lambda$ agrees as proved in Section VII. Equation (A 8) becomes by division with u_{ave} and introduction of Re^+ (A 5, A 6)

$$Q_1 = \frac{Re^+}{Re} \left(\frac{1}{\kappa} \ln Re^+ + B - \frac{3}{2\kappa} \right) = 1. \tag{A 9}$$

Princeton Superpipe data[13,14] for $Re = 3.0 \times 10^6$ with three parameters $Re^+ = 1.0 \times 10^5$ (like Re rounded by the author), $\kappa = 0.391$ and $B = 4.34$ yield $Q_1 = 0.998$ (–0.2 %), a valuable test.

Determined from the pressure drop in the pipe[14] (instead from τ_{wall}) is the wall friction velocity $u_\tau = 23.5 \text{ m/s}$. From Re^+ follows with $\nu = 1.55 \times 10^{-5} \text{ m}^2/\text{s}$ and $a = 6.45 \times 10^{-2} \text{ m}$

$$u_\tau = Re^+ \nu / a = 24.0 \text{ m/s}, \tag{A 10}$$

$$u_{\text{ave}} = u_\tau Re / Re^+ = 720 \text{ m/s}. \tag{A 11}$$

From Re follows

$$v_{\text{ave}} = Re\, \nu / a = 720 \text{ m/s} = u_{\text{ave}}. \tag{A 12}$$

The normalized turbulent effective velocity is analogous to $V_z(\xi)$ (12) with one known parameter $\beta a = 82.94$

$$V_z(\xi) = \frac{1}{\Phi_B(\beta a)} \left\{ 1 - \frac{I_0(\beta a \xi)}{I_0(\beta a)} \right\}. \tag{A 13}$$

For comparison the dimensional logarithmic velocity $u(y)$ (A 1) will be normalized by a and u_{ave}, so that

$$\frac{u(y)}{u_{\text{ave}}} = \frac{u_\tau}{u_{\text{ave}}} \left(\frac{1}{\kappa} \ln \frac{a u_\tau}{\nu} \frac{y}{a} + B \right), \tag{A 14}$$

$$W_z(\eta) = \frac{u(y)}{u_{ave}} = \frac{Re^+}{Re}\left(\frac{1}{\kappa}\ln Re^+\eta + B\right), \tag{A 15}$$

$$W_z(\eta) = \frac{Re^+}{Re}U^+, \tag{A 16}$$

$$\eta = \frac{y}{a} = \frac{Y^+}{Re^+};\ \xi = \frac{r}{a} = 1-\eta. \tag{A 17}$$

Figure A1a shows in linear axes $W_z(\eta)$ and $V_z(\xi)$ for $Re = 3.0\times10^6$, $\beta a = 82.94$, with steep slopes near the wall. For $\eta > 0.1$ is $V_z(\xi) \approx 1.025$ allmost constant, whereas $W_z(\eta)$ increases to $W_{axis} = 1.126$.

In figure A1a is included particularly for $Re \to \infty$ the constant velocity $V_z = 1$. This generally accepted solution is applied in Section IV and V. It is experimentally verified by the hydrogen-bubble visualization quoted in Section III.

Figure A1b displays W_z in semilogarithmic axes [corresponding to Fig. 4 of Ref. 13] as a straight line from $\eta_0 = 1.83_2\times10^{-6}$, $W_z = 0$, up to $\eta = 1$, $W_z = W_{axis}$, with three intersections at $\eta_1 = 1.83_6\times10^{-6}$, $W_z = V_z = 1.52\times10^{-4}$,

$\eta_2 = 1.79\times10^{-2}$, $W_z = V_z = 7.83\times10^{-1}$,

$\eta_3 = 3.06\times10^{-1}$, $W_z = V_z = 1.025 \approx V_{axis}$.

Figures A1c and A1d present the derivatives

$$\frac{dW_z(\eta)}{d\eta} = \frac{Re^+}{Re}\frac{1}{\kappa\eta}, \tag{A 18}$$

$$\frac{dV_z(\xi)}{d\xi} = \frac{\beta a}{\Phi_B(\beta a)}\frac{I_1(\beta a\xi)}{I_0(\beta a)}. \tag{A 19}$$

Both decrease near the wall, for $\eta > 0.1$ they approach zero, for $\eta = 1$ is $\left(dV_z/d\xi\right)_{axis} = 0$ exact.

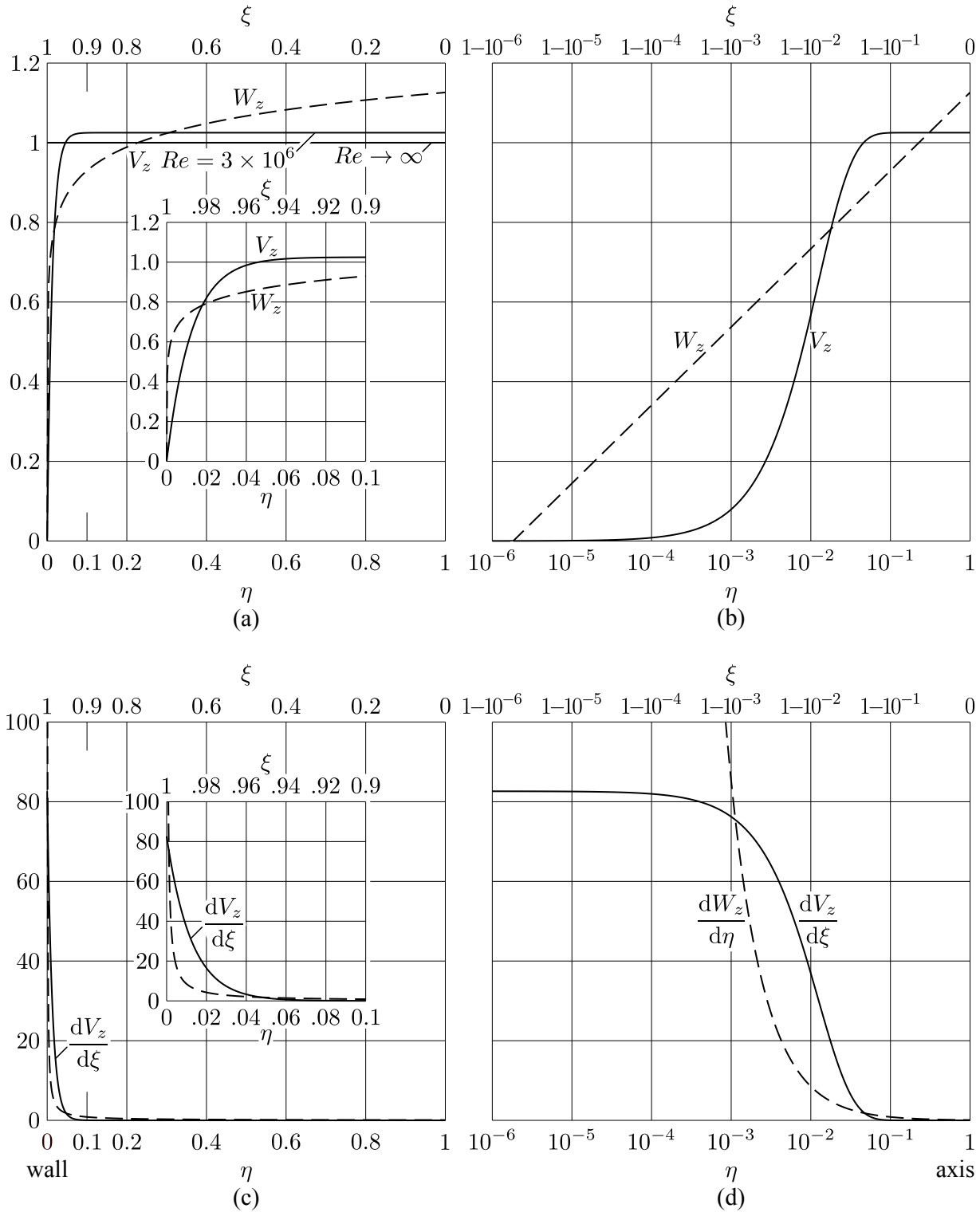

Fig A1. Comparison of logarithmic velocity $W_z(\eta)$ with effective velocity $V_z(\xi)$ for $Re = 3.0 \times 10^6$.

The averages of the different velocities $W_z(\eta)$ and $V_z(\xi)$ are equal:

$$Q_W = 2\int_{\eta=0}^{1} W_z(\eta)(1-\eta)\,d\eta = 1, \tag{A 20}$$

$$Q_V = 2\int_{\xi=0}^{1} V_z(\xi)\xi\,d\xi = 1. \tag{A 21}$$

Considerable differences appear at the wall and at the axis of the pipe:

$$\text{at } \eta = 0,\ W_{wall} = -\infty,\quad \left(\frac{dW_z}{d\eta}\right)_{wall} = \infty; \tag{A 22}$$

$$\text{at } \xi = 1,\ V_{wall} = 0,\quad \left(\frac{dV_z}{d\xi}\right)_{wall} = 82.63; \tag{A 23}$$

$$\text{at } \eta = 1,\ W_{axis} = 1.126,\ \left(\frac{dW_z}{d\eta}\right)_{axis} = 8.525\times10^{-2} \neq 0; \tag{A 24}$$

$$\text{at } \xi = 0,\ V_{axis} = 1.025,\ \left(\frac{dV_z}{d\xi}\right)_{axis} = 0 \text{ exact.} \tag{A 25}$$

Physics demands at the wall non-slip and finite shear-stress, at the axis flat profiles with derivatives $(dV_z/d\xi)_{axis} = 0$ in accordance with figure 1 for all Reynolds numbers Re, not only in restricted regions. Consequently Pitot probes should yield effective velocities by adequate calibration.

All physical criteria have to be fulfilled. Well founded for hyperlaminar and turbulent viscous pipe flows are the effective velocities V_z as symmetric solutions of the extended Navier-Stokes equation valid in cylindrical coordinates from axis to wall over the entire range of Reynolds numbers with respective adherence lengths in agreement with the experiments, alltogether thanks to Ohmic friction.

ACKNOWLEDGEMENTS

The present approach was initiated by investigations on flows of cylindrical symmetry while the author was working in the Departamento de Física, Facultade de Ciências e Tecnologia, Universidade do Algarve, Faro, Portugal (1991-1996). The project could be accomplished with the support of IBM Research – Zurich, Switzerland. Cordial thanks for the efficient cooperation are due to Charlotte Bolliger, Mário Freitas, José António Rodrigues, Christopher Sciacca. Georg Jaggi and Sebastian Jaggi deserve special recognition for the construction of equipment and constant succor.

REFERENCES

[1] O. Reynolds, "An Experimental Investigation of the Circumstances wich determine whether the Motion of Water shall be Direct or Sinuous, and of the Law of Resistance in Parallel Channels," Phil. Trans. R. Soc. Lond. 174, 935 (1883).

[2] H. Schlichting and K. Gersten, "Boundary Layer Theory, " 8th ed., Springer, New York (2000).

[3] F. M. White, "Viscous Fluid Flow, " 3rd ed., Mc Graw-Hill International Edition (2006).

[4] R. R. Kerswell, "Recent progress in understanding the transition to turbulence in a pipe," Nonlinearity 18, R17 (2005).

[5] A. P. Willis, J. Peixinho, R. R. Kerswell and T. Mullin, "Experimental and theoretical progress in pipe flow transition," Phil. Trans. R. Soc. A 366, 2671, (2008).

[6] T. Mullin, "Experimental Studies of Transition to Turbulence in a Pipe," Annu. Rev. Fluid Mech. 43:1 (2011).

[7] J. Kim, "Progress in pipe and channel flow turbulence, 1961-2011," Journal of Turbulence 13, N45 (2012).

[8] C. W. Benthem and R. Kronig, "The anomalus skin effect and the reflectivity of metals," Physica 20, 293 (1954).

[9] R. Jaggi, "Electron-fluid model for dc size effect," J. Appl. Phys. 69, 816 (1991).

[10] R. Jaggi, "Size-Effects in Hydrodynamics," Helv. Phys. Acta 69, Separanda 1, 13 (1996).

[11] B. J. McKeon, C. J. Swanson, M. V. Zagarola, R. J. Donnelly and A. J. Smits, "Friction factors for smooth pipe flow," J. Fluid Mech. 511, 41 (2004).

[12] C. J. S. Swanson, B. Julian, G. G. Ihas and R. J. Donnelly, "Pipe flow measurements over a wide range of Reynolds numbers using liquid helium and various gases," J. Fluid Mech. 461, 51 (2002).

[13] M. Hultmark, M. Vallikivi, S. C. Bailey and A. J. Smits, "Turbulent Pipe Flow at Extreme Reynolds Numbers," Phys. Rev. Lett. 108, 09451 (2012).

[14] I. Marusic, J. P. Monty, M. Hultmark and A. J. Smits, "On the logarithmic region in wall turbulence," J. Fluid Mech. 716, R3 (2013).

Jetzt folgen nur Bruchstrichversuche.

$\partial p / \partial z = -p_{\mathrm{A}} / L$ $\partial p/\partial z = -p_{\mathrm{A}}/L$